Implementation of Oxygen Enhanced Magnetic Resonance Imaging (OE-MRI) and a Pilot Genomic Study of Hypoxia in Bladder Cancer Xenografts

Shabbir, Rekaya ; Telfer, Brian; Dickie, Ben ; Reardon, Mark; Babur, Muhammad ; Williams, Kaye ; Choudhury, Ananya ; West, Catharine; Smith, Tim

Cancer Genomics & Proteomics

DOI:
10.21873/cgp.20455

Published: 27/06/2024

Publisher's PDF, also known as Version of record

CANCER GENOMICS & PROTEOMICS *21*: 380-387 (2024)
doi:10.21873/cgp.20455

Implementation of Oxygen Enhanced Magnetic Resonance Imaging (OE-MRI) and a Pilot Genomic Study of Hypoxia in Bladder Cancer Xenografts

REKAYA SHABBIR[1], BRIAN A. TELFER[2], BEN DICKIE[3], MARK REARDON[1], MUHAMMAD BABUR[4], KAYE WILLIAMS[5], CATHARINE M.L. WEST[1], ANANYA CHOUDHURY[1,6] and TIM A.D. SMITH[1,7]

[1]*Division of Cancer Sciences, The University of Manchester, Manchester, U.K.;*
[2]*Faculty Office, Faculty of Biology, Medicine and Health, University of Manchester, Manchester, U.K.;*
[3]*Division of Informatics, Imaging & Data Sciences, Faculty of Biology, Medicine and Health, The University of Manchester, Manchester, U.K.;*
[4]*Faculty Office Administration, Faculty of Biology, Medicine and Health, The University of Manchester, Manchester, U.K.;*
[5]*Division of Pharmacy & Optometry, School of Health Sciences, Faculty of Biology, Medicine and Health, The University of Manchester, Manchester, U.K.;*
[6]*The Christie Hospitals NHS Foundation Trust, Manchester, U.K.;*
[7]*Nuclear Futures Institute, School of Computer Science and Engineering, Bangor University, Bangor, U.K.*

Abstract. *Background/Aim: Patients with hypoxic bladder cancer benefit from hypoxia modification added to radiotherapy, but no biomarkers exist to identify patients with hypoxic tumours. We, herein, aimed to implement oxygen-enhanced MRI (OE-MRI) in xenografts derived from muscle-invasive bladder cancer (MIBC) for future hypoxia biomarker discovery work; and generate gene expression data for future biomarker discovery. Materials and Methods: The flanks of female CD-1 nude mice inoculated with HT1376 MIBC cells. Mice with small (300 mm^3) or large (700 mm^3) tumours were imaged, breathing air then 100% O_2, 1 h post injection with pimonidazole in an Agilant 7T 16cm bore magnet interfaced to a Bruker Avance III console with a T2-TurboRARE sequence using a dynamic MPRAGE acquisition. Dynamic Spoiled Gradient Recalled Echo images were acquired for 5 min, with 0.1mmol/kg Gd-DOTA (Dotarem, Guerbet, UK) injected after 60 s (1 ml/min). Voxel size and field of view of dynamic contrast enhanced (DCE)-MRI and OE-MRI scans were matched. The voxels considered as perfused with significant post-contrast enhancement ($p<0.05$) in DCE-MRI scans and tissue were further split into pOxyE (normoxic) and pOxyR (hypoxic) regions. Tumours harvested in liquid N_2, sectioned, RNA was extracted and transcriptomes analysed using Clariom S microarrays. Results: Imaged hypoxic regions were greater in the larger versus smaller tumour. Expression of known hypoxia-inducible genes and a 24 gene bladder cancer hypoxia score were higher in pimonidazole-high versus -low regions: CA9 ($p=0.012$) and SLC2A1 ($p=0.012$) demonstrating expected transcriptomic behaviour. Conclusion: OE-MRI was successfully implemented in MIBC-derived xenografts. Transcriptomic data derived from hypoxic and non-hypoxic xenograft regions will be useful for future studies.*

Correspondence to: Dr. Tim Smith, Oglesby Cancer Research Centre, 555 Wilmslow Road, Manchester M20 4GJ, U.K. E-mail: tim.smith@bangor.ac.uk

Key Words: Hypoxia, oxygen-enhanced MRI, xenograft, bladder cancer, transcriptome.

Hypoxia is a feature of most solid tumours (1) associated with genomic instability and treatment resistance, particularly to radiotherapy. Improved responses can be achieved by using hypoxia modification during radiotherapy (2). To date, there are no biomarkers in clinical use that identify patients with hypoxic tumours. Hypoxia scores derived from the collective expression of multiple genes can predict benefit from hypoxia modification (3-6). Medical imaging techniques can identify regions within tumours for additional treatment dose and are suitable for serial measurements (7). Two magnetic resonance imaging (MRI)

techniques, oxygen-enhanced MRI (OE-MRI) and Dynamic Contrast Enhanced (DCE-MRI) when combined enable the non-invasive mapping of hypoxia in tumours (8). DCE-MRI identify regions within tumours that are perfused whilst OE-MRI show regions that utilise oxygen.

The aim of the study was to assist hypoxia target discovery work by: a) implementing OE-MRI/DCE-MRI in a xenograft model of bladder cancer and (b) using laser dissected tissue from pimonidazole demarcated regions in the xenograft model to produce a publicly available gene expression database.

Materials and Methods

Figure 1 shows a schematic of the xenograft model preparation, imaging, and RNA analysis.

Bladder cancer cell culture. HT1376 (ATCC, Virginia) MIBC cells were cultured in Eagle's Minimum Essential Medium (EMEM) (Sigma-Aldrich, St. Louis, MO, USA) supplemented with 10% Foetal Bovine Serum (FBS) (Gibco, Thermo-Fisher Scientific, Waltham, MA, USA). The cells were screened for mycoplasma and Murine Hepatitis Virus (MHV) prior to implantation into mice.

Animal handling procedures. The experiment was conducted on 8-week-old female CD-1 nude mice (n=2), body weight 20 g purchased from (Charles River Laboratories, Wilmington, MA, USA). The mice, housed in cages under an Individually Ventilated Caging (IVC) system, were allowed to acclimatise for 7 days prior to implantation. The mice were fed *ad libitum* with standard mouse diet and water during the experiment. All experiments were carried out under UK Animals (Scientific Procedures) Act 1986, UK Home Office regulations.

HT1376 cell line derived xenograft (CDX) model. Using a 25-gauge needle, HT1367 cells (10^6 cells in 100 µl of phosphate buffered saline) were subcutaneously inoculated into the flanks of female CD nude mice on the lower quadrant, 1 cm from the tail base. This was counted as day zero. Pre-injection sites were swabbed with chlorohexidine wipes and Betadine (iodine) post swabs for sterilisation. The injection was done under isoflurane anaesthesia. Mice were sedated using 3-5% isoflurane for around 5 minutes in total (knockdown and chip implant (ID microchipped to distinguish mice) and cell inoculation. After subcutaneous injection, mice were allowed to fully recover in a warming box if needed and observed every 10-15 min for 1h. They were then returned to their cages and provided with food and water during the study period.

Tumour measurement and monitoring. Tumour volume measurements and weight were recorded every other day using a digital calliper and scale. The tumour volume was calculated using the formula: H×W×L where H is the tumour height, W is the tumour width and L is the tumour length, in mm. Mice were euthanized by a schedule 1 technique when the tumour reached 300 mm^3 (small tumour) and 700 mm^3 (large tumour) in size.

MRI and pathology correlation. One mouse was imaged at tumour size 300 mm^3 and the other at 700 mm^3. Mice had intraperitoneal (*ip*) injections with the hypoxia biomarker pimonidazole (Hypoxyprobe-1-pimo) (60 mg/kg) (Chemicon Ltd, Feltham, UK)

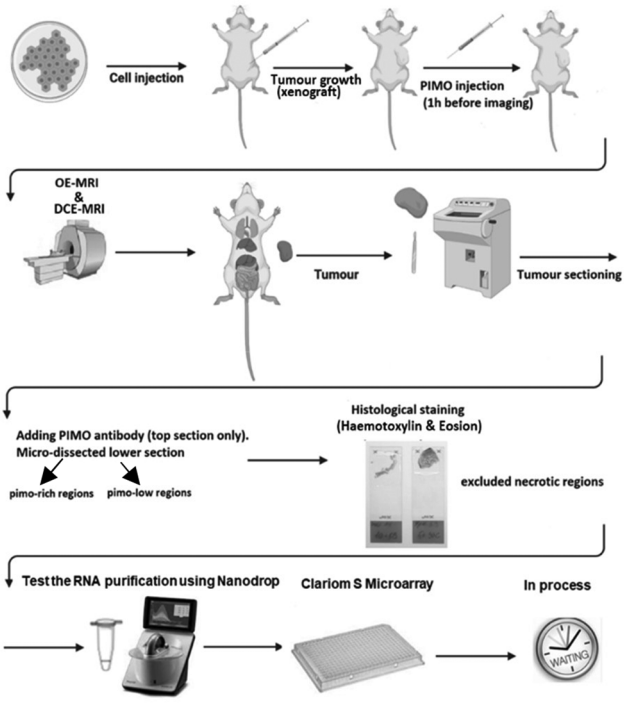

Figure 1. *Schematic of the experimental design for the preparation of the cell line-derived xenografts, imaging, and transcriptional profiling.*

immediately before MRI imaging. The mice were then placed in an Agilant 7T 16cm bore magnet MRI interfaced to a Bruker Avance III. Animals were scanned using T2-TurboRARE, OE-MRI and DCE-MRI. OE-MRI scans were acquired using a dynamic MPRAGE acquisition: TR/TE=6,000/3.10 ms, TI=2,000 ms, voxel size=0.234×0.234×0.5 mm, 30 slices with total duration of 32 min. The OE-MRI acquisition was carried out with the mouse breathing medical air then switched from medical air to 100% O_2 midway through for the remainder of the scanning session. Following OE-MRI, DCE-MRI was performed to determine perfused volume pixel (voxels). Dynamic Spoiled Gradient-Recalled (SPGR) images were acquired for 5 min 52 s (flip angle=30°, TR/TE=10.2/1.9 ms), with 0.1 mmol/kg Gd-DOTA (Dotarem, Guerbet, UK) injected after 60 s at 1ml/min *via* a tail vein cannular, under anaesthesia, during the scan for contrast enrichment. Voxel size and field of view (FOV) of DCE-MRI and OE-MRI scans were matched. The voxels with significant post-contrast enhancement ($p<0.05$) in DCE-MRI scans were classified as perfused. From the perfused voxels, tissue was further split into two sub-regions pOxyE (normoxia) and pOxyR (hypoxia) based on post-contrast enhancement on OE-MRI ($p<0.05$). At the end of the study, mice were euthanised by schedule 1 method and tumours cut in half and frozen in liquid nitrogen.

DCE-MRI image processing and analysis. DCE-MRI (OE-MRI) images were analysed using MATLAB® version R2017a.

Laser capture microdissection (LCM), IHC and histology. Sections were obtained from across the middle of the tumour using a cryostat. Two×4 µm sections were cut for immunohistochemistry

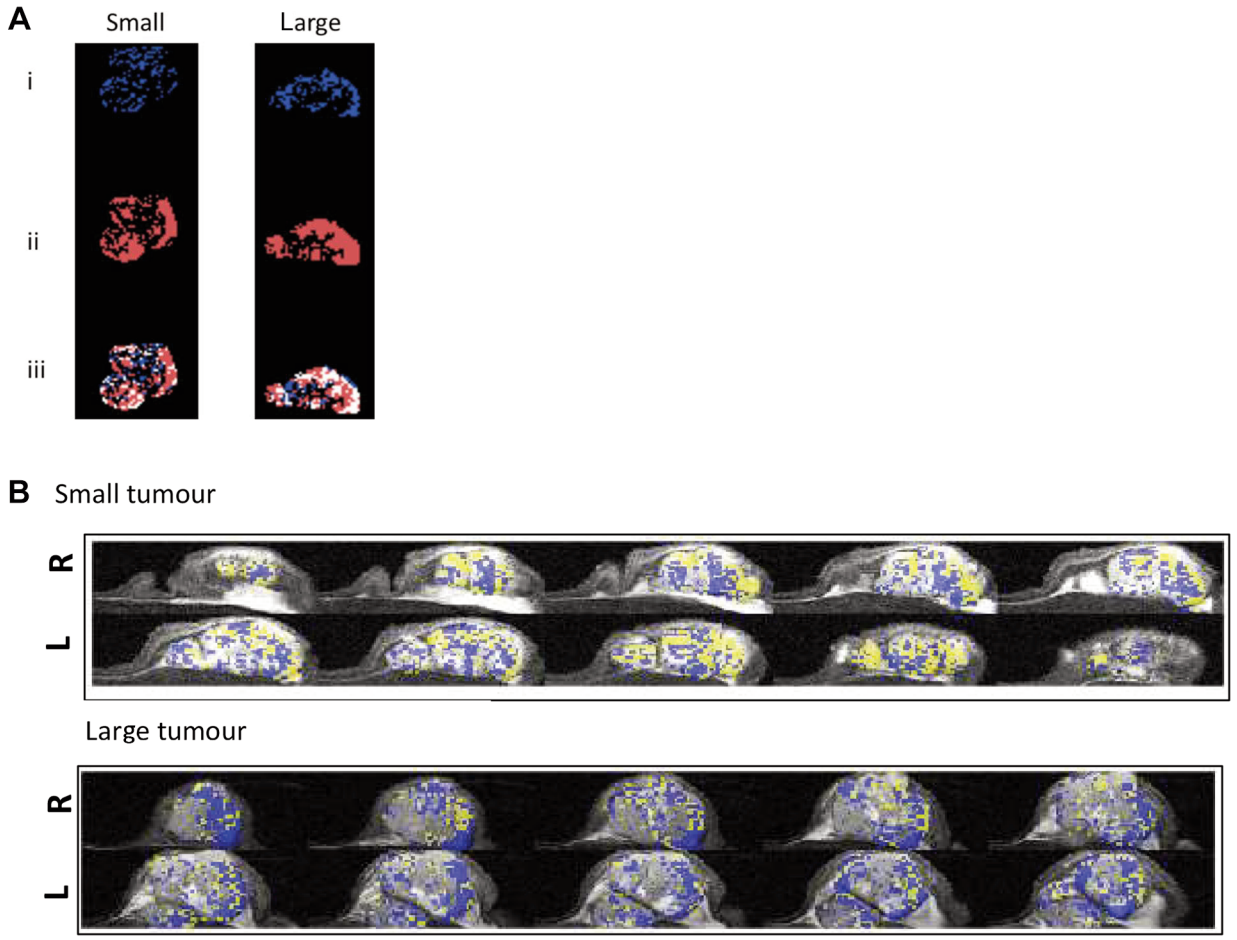

Figure 2. *(A) Regions of oxygen enhancement (i) in blue, perfusion (ii) in red and a Montage (iii) of i and ii illustrating regions of perfusion and oxygen enhancement in white. (B) Montage of images derived by OE-MRI and DCE- MRI for the small tumor and large tumor. Top image in each panel reflects the right side of the tumor and bottom image reflects the left side of the tumor. pOxyE: Perfused normoxic areas (yellow); pOxyR: perfused hypoxic areas (blue); not perfused areas identified (grey).*

(IHC) to localise pimonidazole, and hematoxilyn and eosin (H&E) staining to identify necrotic regions. Further sections (10 μm) were prepared for microdissection using laser capture microdissection (LCM) from pimonidazole-high and pimonidazole-low regions The pimonidazole (Hypoxyprobe Mab-1) antibody was used at a dilution of 1/50 (1.2 μg/ml) to localise pimonidazole in one of the 4 μm sections (Figure 2). Necrotic regions were identified and excluded using the H&E-stained sections.

RNA extraction, sequencing, and Clariom S microarray. RNA from xenograft tissue was extracted following the manufacturer's protocol (Thermo-Fisher, UK). Transcriptomes were generated using Clariom S Affymetrix transcriptome arrays. RNA extracted from the 6 micro-dissected samples were subject to Clariom S analysis using the Clariom S pico HT human assay (Thermo Fisher Scientific). Sample hybridisation on Clariom S arrays was carried out by Yourgene Health (Manchester, UK). Batches of CEL files were GC SST (Signal Space Transformation with probe Guanine cytosine count correction) RNA normalised using Affymetrix.

Array power tools. Microarray analytical tools are available on the Thermo-Fisher website (9). The $\log_2$ summarised gene level expression values generated were batch corrected using the comBat function from the Bioconductor package sva (10). Hypoxia scores were calculated as the median expression of the 24 signature genes (3).

Data sharing. All transcriptomic data from this study are deposited in the GEO repository (Geo@ncbi.nlm.nih.gov) under accession GSE262610.

Results

Identification of oxygen-rich and perfused regions. Figure 2A shows representative slices from OE-MRI (A) and DCE-MRI (B) images of a small and a large bladder cancer xenograft. The montage map (C) identifies regions that are perfused and demonstrate enhanced signal during 100% O_2 breathing (p-OxyE) in white or no enhancement (p-OxyR) in red. Figure 2B

shows montage plots of the perfusion (DCE-MRI) and oxygen-enhancement (OE-MRI) maps in slices from left to middle and from right to middle of the small and large tumour. Regions that are perfused normoxic (pOxy-E) are shown in yellow and regions that are perfused hypoxic (pOxy-R) are shown in blue.

Table I shows the overall levels of normoxia (P-OxyE) and hypoxia (P-OxyR) in the small and large tumour and the proportion of tumours that are necrotic. Both hypoxia and necrosis are higher in the larger compared with the smaller tumour.

Identification of non-necrotic hypoxic and non-hypoxic regions. Figure 3 shows adjacent tumour sections from frozen xenografts subjected to H&E staining (A) and IHC using a pimonidazole antibody (B). Pimonidazole-positive and -negative regions excluding necrotic regions were micro-dissected from contiguous sections to the H&E and pimonidazole-guide slides. Figure 3C shows regions stained with the pimonidazole-antibody in sections immediately adjacent to the upper and lower sections micro-dissected for RNA extraction. The locality of pimonidazole-staining is similar in both indicating that the regions of hypoxia will be consistent though the micro-dissected series of sections. Six regions were micro-dissected, three from pimonidazole-positive and three from pimonidazole-negative regions. The quantity and quality (RIN) of the RNA extracted from micro-dissected tissue from six regions demonstrating pimonidazole-negative (three samples) and pimonidazole-positive (three samples) staining are shown in Table II. RIN >1.4 is considered as a minimal RNA integrity level (9) RIN values were 7.0 and 7.6 for Pimonidazole-rich and Pimonidazole-low samples respectively. These samples were considered acceptable for transcriptomic analysis using Clariom S.

Expression of genes encoding cell surface proteins associated with hypoxia. The expression of known hypoxia associated genes, CA9, SLC2A1 (Glut-1) and VEGFA, shown in Figure 4, were increased in expression in pimonidazole-positive compared with pimonidazole-negative regions.

Hypoxia score (HS) generated using the West 24 gene hypoxia signature. Hypoxia scores (HS) were generated using a 24-gene expression bladder cancer hypoxia signature (3). Figure 5 shows the HS of each (A) individual sample and (A) mean of the pimonidazole-positive (n=3) and pimonidazole-negative (n=3) samples. HS was higher (p=0.0052) in the pimonidazole-positive than in pimonidazole-negative samples.

Table I. *Percentages of the small and large tumour that were perfused*.

	Small tumor	Large tumor
Perfused	73%	48%
Perfused OxyE (normoxic)	49%	24%
Perfused OxyR (hypoxic)	51%	76%
Non-perfused (necrotic)	27%	52%

Normoxic: Perfused with O_2-enhancement; hypoxic: perfused without O_2-enhancement; and not-perfused (necrotic). OxyE, oxygen enhancement; OxyR, no oxygen enhancement.

Discussion

The need for hypoxia biomarkers is exemplified by Spiegelberg *et al*. who found that the failure of phase III trials can be fully explained by lack of patient classification based on tumour hypoxia status (11). Imaging and transcriptomics have been applied to various cancer types (12) for investigations including diagnosis, prognosis, and prediction of extracellular matrix (13) as they provide complementary and potentially mechanistic information. Small animal experiments either preclinical or back translational are essential to understanding and developing novel approaches to characterising cancer. The findings here show that xenografts are convenient models for combined imaging and genomic analysis.

Combined DCE-MRI and OE-MRI developed at the University of Manchester, for the identification of hypoxia has been validated in clinical (14) as well as pre-clinical (15) work. In this study the higher proportion of hypoxia in the larger tumour compared with the smaller demonstrated using OE-MRI/DCE-MRI agrees with other studies (16-20). Necrosis was also higher in the large tumour and was evident in over half the volume in agreement with previous studies reporting on size association with necrotic fraction (18, 19). Several studies have shown that the presence of the necrotic regions in tumours associated with hypoxia (21, 22). Patients with highly necrotic muscle invasive bladder cancer were shown to benefit from carbogen-nicotinamide (CON) modified therapy (21).

Tumour hypoxia induces angiogenesis through up-regulation of VEGF expression. Other mechanisms that enable cancer cells to thrive in hypoxic conditions include up-regulation of cell surface expression of Glut-1 thus increasing glucose uptake to fuel glycolysis and CA9 to reduce the consequent intracellular acidification. Genes encoding the cell surface proteins CA9, Glut-1 and VEGF3 (*CA9*, *SLC2A1* and *VEGF3*), associated with hypoxia (23, 24), were increased in expression in pimonidazole-positive regions. Clinical work has shown that both CA9 and Glut-1 co-localise with pimonidazole in patients with MIBC (23). Studies have demonstrated that overexpression of CA9 and Glut-1 protein in squamous cell Head and Neck Cancer and MIBC is associated with poor response to chemotherapy (22-24).

Glut-1, CA9 and VEGF3 protein expression can readily be detected by IHC. A general disadvantage of IHC is that it

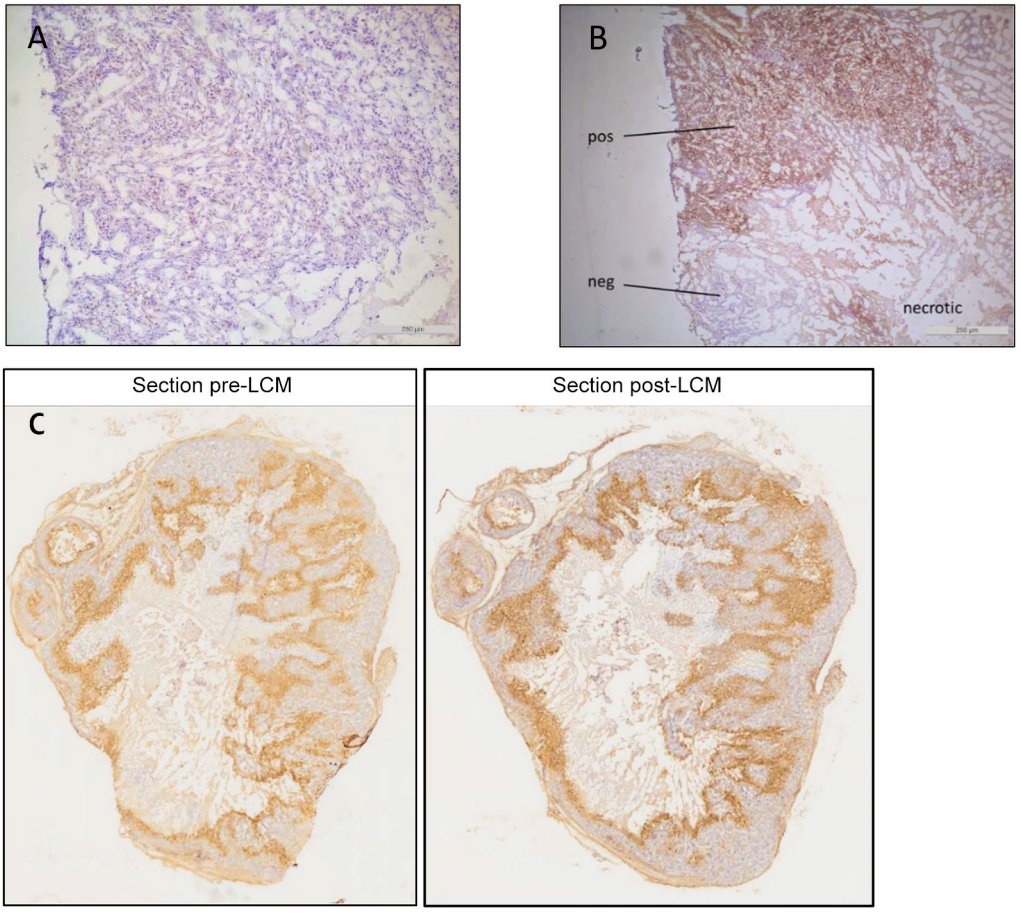

Figure 3. *Identification of necrotic and hypoxic/non-hypoxic regions in adjacent tissue sections. (A) H&E-stained section of xenograft showing region of necrosis and (B) adjacent tumor section subject to immunohistochemistry with pimonidazole antibody showing pimonidazole-positive (hypoxic) and pimonidazole-negative (non-hypoxic) regions. (C) Sections above and below micro-dissected series of sections. RNA extraction from xenografted tumours.*

Table II. *Concentration and quality of RNA extracted from tissue micro-dissected contiguous sections from 3 pimonidazole-positive and 3 pimonidazole-negative regions.*

		RNA concentration (ng/μl)			
Samples	n	Nanodrop	Qubit	RIN	Vol (μl)
Pimonidazole-positive	3	49±41	57±54	7.0±1	10
Pimonidazole-negative	3	29±12	17±7	7.6±0.6	10

RIN, RNA integrity number.

does not give an overall measure of hypoxia in the tumour. However, gene hypoxic status generated using gene expression signatures (3) demonstrate low levels of intra-tumour heterogeneity (25) suggesting that robust tumour characterisation at the gene expression level can be derived from individual samples. The 24-gene bladder cancer hypoxia signature derived from a candidate panel of hypoxia-responsive genes and refined by prognostication in bladder cancer patient cohorts has also been shown to be predictive of benefit from hypoxia modification (2). This study has demonstrated that the signature is sensitive to hypoxia in *in vivo* model.

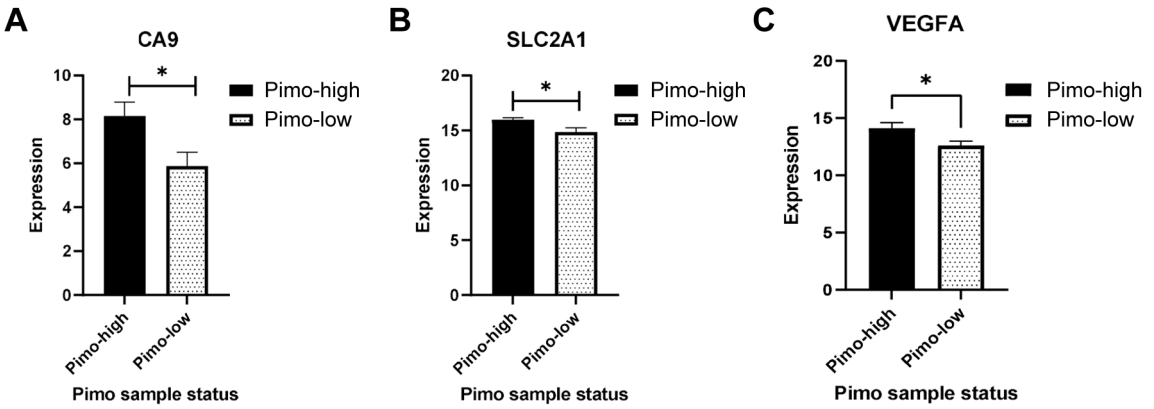

Figure 4. *Expression of genes associated with cell surface proteins of hypoxia. Expression of (A) CA9, (B) SLC2A1 and (C) VEGFA in pimonidazole-positive and pimonidazole-negative regions. *p<0.05, ***p<0.001. Pimo: Pimonidazole.*

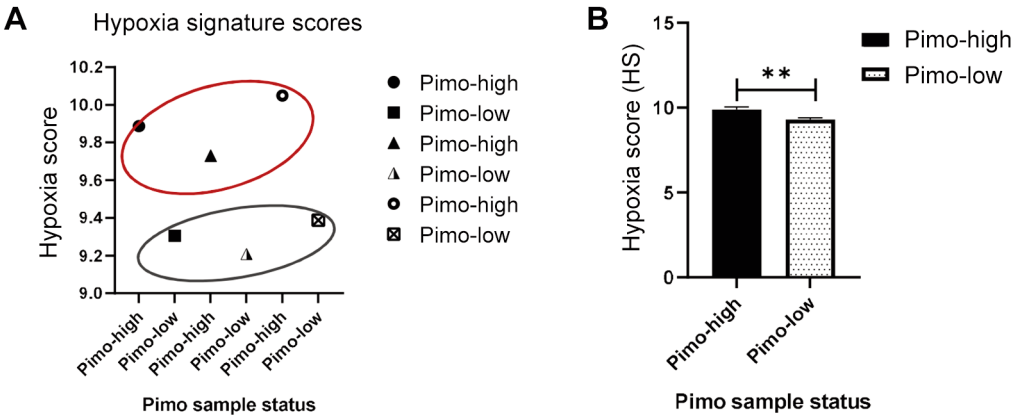

Figure 5. *Hypoxia scores (HS) generated from RNA extracted from pimonidazole-positive and pimonidazole-negative samples. (A) The HS in samples from each pimonidazole-positive and pimonidazole-negative sample. (B) Mean and SD of HS differences (**p<0.0052) between pimonidazole-positive and pimonidazole-negative. Pimo: Pimonidazole.*

This work does have the obvious limitation in sampling from just two tumours.

However multiple sampling of high and low-pimonidazole regions (n=3 of each) from one tumour demonstrated up-regulation of hypoxia-sensitive genes CA9 and GLUT-1 validating the data set for exploration of other gene-expression hypoxia biomarkers and mechanisms underlying the hypoxia-associated phenotype. Single samples from multiple mice increase the potential for genetic variability between replicates and the requirement for many more mice. Genomic analysis facilitates patient stratification and predicts patent outcome. Combining hypoxia imaging techniques with gene expression signatures has the potential to provide robust biomarkers of tumour hypoxia leading to improved patient treatment selection (26). This work has demonstrated that data from MRI based imaging techniques can be acquired alongside gene expression in xenograft models to assist is the development of biomarkers.

Funding

Funding from the Saudi Arabian Bureau of Culture is gratefully acknowledged.

Conflicts of Interest

The Authors declare no conflicts of interest.

Authors' Contributions

Manuscript preparation: RS, TADS; Edited and approved manuscript; All authors, Designed study TADS, KW, CW; MRI measurements and data analysis: BD, MB; *In vivo* model development BT and RS; Sample preparation and transcriptomics RS and MR.

Acknowledgements

The University of Manchester Core Facility for preparation of sections, micro-dissection, and RNA extraction.

References

1 Telarovic I, Wenger RH, Pruschy M: Interfering with tumor hypoxia for radiotherapy optimization. J Exp Clin Cancer Res 40(1): 197, 2021. DOI: 10.1186/s13046-021-02000-x

2 Hoskin PJ, Rojas AM, Bentzen SM, Saunders MI: Radiotherapy with concurrent carbogen and nicotinamide in bladder carcinoma. J Clin Oncol 28(33): 4912-4918, 2010. DOI: 10.1200/JCO.2010.28.4950

3 Yang L, Taylor J, Eustace A, Irlam JJ, Denley H, Hoskin PJ, Alsner J, Buffa FM, Harris AL, Choudhury A, West CM: A gene signature for selecting benefit from hypoxia modification of radiotherapy for high-risk bladder cancer patients. Clin Cancer Res 23(16): 4761-4768, 2017. DOI: 10.1158/1078-0432.CCR-17-0038

4 Eustace A, Mani N, Span PN, Irlam JJ, Taylor J, Betts GN, Denley H, Miller CJ, Homer JJ, Rojas AM, Hoskin PJ, Buffa FM, Harris AL, Kaanders JH, West CM: A 26-gene hypoxia signature predicts benefit from hypoxia-modifying therapy in laryngeal cancer but not bladder cancer. Clin Cancer Res 19(17): 4879-4888, 2013. DOI: 10.1158/1078-0432.CCR-13-0542

5 Forker LJ, Bibby B, Yang L, Lane B, Irlam J, Mistry H, Khan M, Valentine H, Wylie J, Shenjere P, Leahy M, Gaunt P, Billingham L, Seddon BM, Grimer R, Robinson M, Choudhury A, West C: Technical development and validation of a clinically applicable microenvironment classifier as a biomarker of tumour hypoxia for soft tissue sarcoma. Br J Cancer 128(12): 2307-2317, 2023. DOI: 10.1038/s41416-023-02265-3

6 Smith TAD, West CML, Joseph N, Lane B, Irlam-Jones J, More E, Mistry H, Reeves KJ, Song YP, Reardon M, Hoskin PJ, Hussain SA, Denley H, Hall E, Porta N, Huddart RA, James ND, Choudhury A: A hypoxia biomarker does not predict benefit from giving chemotherapy with radiotherapy in the BC2001 randomised controlled trial. EBioMedicine 101: 105032, 2024. DOI: 10.1016/j.ebiom.2024.105032

7 Grosu AL, Souvatzoglou M, Röper B, Dobritz M, Wiedenmann N, Jacob V, Wester HJ, Reischl G, Machulla HJ, Schwaiger M, Molls M, Piert M: Hypoxia imaging with FAZA-PET and theoretical considerations with regard to dose painting for individualization of radiotherapy in patients with head and neck cancer. Int J Radiat Oncol Biol Phys 69(2): 541-551, 2007. DOI: 10.1016/j.ijrobp.2007.05.079

8 O'Connor JP, Boult JK, Jamin Y, Babur M, Finegan KG, Williams KJ, Little RA, Jackson A, Parker GJ, Reynolds AR, Waterton JC, Robinson SP: Oxygen-enhanced MRI accurately identifies, quantifies, and maps tumor hypoxia in preclinical cancer models. Cancer Res 76(4): 787-795, 2016. DOI: 10.1158/0008-5472.CAN-15-2062

9 Microarray analysis tools. Available at: https://www.thermofisher.com/uk/en/home/life-science/microarray-analysis/microarray-analysis-partners-programs/affymetrix-developers-network.html [Last accessed on September 9, 2023]

10 Leek JT, Johnson WE, Parker HS, Jaffe AE, Storey JD: The sva package for removing batch effects and other unwanted variation in high-throughput experiments. Bioinformatics 28(6): 882-883, 2012. DOI: 10.1093/bioinformatics/bts034

11 Spiegelberg L, Houben R, Niemans R, de Ruysscher D, Yaromina A, Theys J, Guise CP, Smaill JB, Patterson AV, Lambin P, Dubois LJ: Hypoxia-activated prodrugs and (lack of) clinical progress: The need for hypoxia-based biomarker patient selection in phase III clinical trials. Clin Transl Radiat Oncol 15: 62-69, 2019. DOI: 10.1016/j.ctro.2019.01.005

12 Li S, Zhou B: A review of radiomics and genomics applications in cancers: the way towards precision medicine. Radiat Oncol 17(1): 217, 2022. DOI: 10.1186/s13014-022-02192-2

13 Kang W, Qiu X, Luo Y, Luo J, Liu Y, Xi J, Li X, Yang Z: Application of radiomics-based multiomics combinations in the tumor microenvironment and cancer prognosis. J Transl Med 21(1): 598, 2023. DOI: 10.1186/s12967-023-04437-4

14 Dubec MJ, Buckley DL, Berks M, Clough A, Gaffney J, Datta A, McHugh DJ, Porta N, Little RA, Cheung S, Hague C, Eccles CL, Hoskin PJ, Bristow RG, Matthews JC, van Herk M, Choudhury A, Parker GJM, McPartlin A, O'Connor JPB: First-in-human technique translation of oxygen-enhanced MRI to an MR Linac system in patients with head and neck cancer. Radiother Oncol 183: 109592, 2023. DOI: 10.1016/j.radonc.2023.109592

15 Salem A, Little RA, Latif A, Featherstone AK, Babur M, Peset I, Cheung S, Watson Y, Tessyman V, Mistry H, Ashton G, Behan C, Matthews JC, Asselin MC, Bristow RG, Jackson A, Parker GJM, Faivre-Finn C, Williams KJ, O'Connor JPB: Oxygen-enhanced MRI is feasible, repeatable, and detects radiotherapy-induced change in hypoxia in xenograft models and in patients with non–small cell lung cancer. Clin Cancer Res 25(13): 3818-3829, 2019. DOI: 10.1158/1078-0432.CCR-18-3932

16 Shibamoto Y, Yukawa Y, Tsutsui K, Takahashi M, Abe M: Variation in the hypoxic fraction among mouse tumors of different types, sizes, and sites. Jpn J Cancer Res 77(9): 908-915, 1986.

17 Gerweck LE, Zaidi ST, Zietman A: Multivariate determinants of radiocurability I: Prediction of single fraction tumor control doses. Int J Radiat Oncol Biol Phys 29(1): 57-66, 1994. DOI: 10.1016/0360-3016(94)90226-7

18 Hildingsson S, Gebre-Medhin M, Zschaeck S, Adrian G: Hypoxia in relationship to tumor volume using hypoxia PET-imaging in head & neck cancer - A scoping review. Clin Transl Radiat Oncol 36: 40-46, 2022. DOI: 10.1016/j.ctro.2022.06.004

19 Belli JA, Andrews JR: Relationship between tumor growth and radiosensitivity. J Natl Cancer Inst 31(3): 689-703, 1963. DOI: 10.1093/jnci/31.3.689

20 Stanley JA, Shipley WU, Steel GG: Influence of tumour size on hypoxic fraction and therapeutic sensitivity of Lewis lung tumour. Br J Cancer 36(1): 105-113, 1977. DOI: 10.1038/bjc.1977.160

21 Eustace A, Irlam JJ, Taylor J, Denley H, Agrawal S, Choudhury A, Ryder D, Ord JJ, Harris AL, Rojas AM, Hoskin PJ, West CM: Necrosis predicts benefit from hypoxia-modifying therapy in patients with high risk bladder cancer enrolled in a phase III randomised trial. Radiother Oncol 108(1): 40-47, 2013. DOI: 10.1016/j.radonc.2013.05.017

22 Song YP, Mistry H, Irlam J, Valentine H, Yang L, Lane B, West C, Choudhury A, Hoskin PJ: Long-term outcomes of radical radiation therapy with hypoxia modification with biomarker discovery for stratification: 10-year update of the BCON

(bladder carbogen nicotinamide) phase 3 randomized trial (ISRCTN45938399). Int J Radiat Oncol Biol Phys 110(5): 1407-1415, 2021. DOI: 10.1016/j.ijrobp.2021.03.001

23 Hoskin PJ, Sibtain A, Daley FM, Wilson GD: GLUT1 and CAIX as intrinsic markers of hypoxia in bladder cancer: relationship with vascularity and proliferation as predictors of outcome of ARCON. Br J Cancer 89(7): 1290-1297, 2003. DOI: 10.1038/sj.bjc.6601260

24 Koukourakis MI, Giatromanolaki A, Sivridis E, Simopoulos K, Pastorek J, Wykoff CC, Gatter KC, Harris AL: Hypoxia-regulated carbonic anhydrase-9 (CA9) relates to poor vascularization and resistance of squamous cell head and neck cancer to chemoradiotherapy. Clin Cancer Res 7(11): 3399-3403, 2001.

25 Smith TAD, Lane B, More E, Valentine H, Lunj S, Abdelkarem OA, Irlam-Jones J, Shabbir R, Vora S, Denley H, Reeves KJ, Hoskin PJ, Choudhury A, West CML: Comparison of multiple gene expression platforms for measuring a bladder cancer hypoxia signature. Mol Med Rep 26(2): 261, 2022. DOI: 10.3892/mmr.2022.12777

26 Liu Z, Zhang J: Radiogenomics correlation between MR imaging features and mRNA-based subtypes in lower-grade glioma. BMC Neurol 20(1): 259, 2020. DOI: 10.1186/s12883-020-01838-6

Received April 5, 2024
Revised May 8, 2024
Accepted May 20, 2024